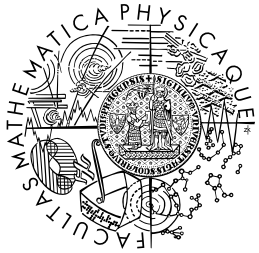

FACULTY
OF MATHEMATICS
AND PHYSICS
Charles University

Summary of doctoral thesis

DAVID EINŠPIGEL

TIME-DOMAIN MODELLING OF GLOBAL BAROTROPIC OCEAN TIDES

Department of geophysics

Supervisor:	prof. RNDr. Zdeněk Martinec, DrSc.
Study programme:	Physics
Study branch:	Geophysics

Prague 2017

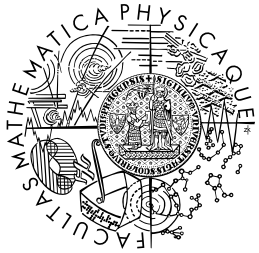

MATEMATICKO-FYZIKÁLNÍ
FAKULTA
Univerzita Karlova

Autoreferát dizertační práce

DAVID EINŠPIGEL

MODELOVÁNÍ GLOBÁLNÍCH BAROTROPNÍCH OCEÁNSKÝCH SLAPŮ V ČASOVÉ OBLASTI

Katedra geofyziky

Školitel: prof. RNDr. Zdeněk Martinec, DrSc.

Studijní program: Fyzika

Studijní obor: Geofyzika

Praha 2017

Dizertace byla vypracována na základě výsledků získaných v letech 2012–2016 během doktorandského studia na Katedře geofyziky MFF UK a School of Cosmic Physics, Dublin Institute for Advanced Studies.

Dizertant:
Mgr. David Einšpigel
School of Cosmic Physics, Dublin Institute for Advanced Studies
5 Merrion Square, Dublin 2, Ireland

Školitel:
Prof. RNDr. Zdeněk Martinec, DrSc.
School of Cosmic Physics, Dublin Institute for Advanced Studies
5 Merrion Square, Dublin 2, Ireland
Katedra geofyziky MFF UK
V Holešovičkách 2, 180 00 Praha 8

Oponenti:
Doc. RNDr. Ctirad Matyska, DrSc.
Katedra geofyziky MFF UK
V Holešovičkách 2, 180 00 Praha 8

Roger Haagmans
European Space Research and Technology Centre
Keplerplaan 1, NL-2201 AZ, Noordwijk, The Netherlands

Předsedkyně oborové rady:
Doc. RNDr. Hana Čížková, Ph.D.
Katedra geofyziky MFF UK
V Holešovičkách 2, 180 00 Praha 8

Autoreferát byl odeslán dne

Obhajoba dizertace se koná dne 4.5.2017 v 10:00 hodin před komisí pro obhajoby dizertačních prací v oboru Geofyzika v budově MFF UK, Ke Karlovu 3, Praha 2, v místnosti M252.

S dizertací je možno se seznámit v PGS MFF UK, Ke Karlovu 3, Praha 2.

Contents

Introduction

Ocean tides are an important phenomenon which has a significant impact on the entire Earth system. Therefore, precise ocean tide modelling is needed for many geophysical and geodetic applications. One of the most important application of ocean tide models is removing tidal signals from various measurements, for example satellite altimetry or gravimetry, so any non-tidal signal can be studied (e.g., Fu and Cazenave, 2001; Seeber, 2003; Visser et al., 2010). Among other applications of ocean tide models, we can mention dissipation of tidal energy, generation of internal tides and mixing of the oceans (e.g., Vlasenko et al., 2005; Arbic et al., 2010; Müller et al., 2012; Taguchi et al., 2014), variations of the Earth's rotation due to tides (e.g., Weis, 2006; Schindelegger et al., 2016) or the induced magnetic field generated by motions of conductive seawater in the main geomagnetic field (e.g., Tyler et al., 2003; Kuvshinov and Olsen, 2005; Sabaka et al., 2015; Velímský et al., 2016).

Traditionally, ocean tides have been modelled in frequency domain with forcing of selected tidal constituents, e.g., M_2, S_2, O_1, K_1, etc. This is the case of the historical models from 70s and 80s but also some modern hydrodynamical models, e.g., STM-1B (Hill et al., 2011) and assimilative models, e.g., FES (Lyard et al., 2006; Carrère et al., 2012), HAMTIDE (Zahel, 1995; Taguchi et al., 2014) and TPXO (Egbert et al., 1994; Egbert and Erofeeva, 2002). Such an approach is natural since ocean tides are primarily composed of handful of peri-

odical or quasi-periodical signals, however, it neglects non-linearities of ocean dynamics. It means that compound tides, e.g., M_4, MS_4, MN_4, etc., which are generated mainly on continental shelves by non-linear interactions of astronomical tidal components, can not be predicted by frequency-domain models. Although, we should note that the compound tides are still modelled in FES by an iterative approach, however at the price of expensive computational costs (Carrère et al., 2012). Apart from the compound tides, another non-linearity is caused by the energy dissipation due to the friction at the sea bottom which is usually parameterized in a quadratic form. Therefore, an alternative parameterization has to be implemented in frequency-domain models. STM-1B uses an iterative scheme while the assimilative models include linearised bottom drag terms.

In this thesis, we apply an alternative approach. We deal with ocean tide modelling in time domain with the full lunisolar forcing. This means that all tidal components, including the compound tides, are modelled simultaneously. Of course, this is not a completely novel approach. Several high-quality time-domain models have been developed, e.g., OTIS (Egbert et al., 2004) which is, however, forced by selected tidal components only; TiME (Weis et al., 2008) with the full astronomical forcing but without a parameterization of the important internal tide drag; or baroclinic models STORMTIDE (Müller et al., 2012) and HYCOM (Arbic et al., 2010) which combine ocean circulation and tides.

The model presented in this thesis is called "DEBOT" (David Einšpigel Barotropic Ocean Tides) and incorporates the full lunisolar forcing given by the astronomical tidal potential of the second and third order which is computed from ephemerides, i.e., actual positions of the Moon and Sun. DEBOT has been built up "from scratch" and has been developed since the author's master studies, see the author's master thesis Einšpigel (2012). The model has substantially changed since Einšpigel (2012) from a rather general shallow-water model to a realistic ocean tide model. The derivation of the shallow-water equations, which are a base of the model, has been revised and an original semi-implicit time-stepping scheme has been replaced by a generalized forward-backward scheme. And most importantly, a data assimilation scheme has been developed and implemented in the time-domain model. As a consequence, DEBOT has two modes: the purely hydrodynamical mode, denoted as "DEBOT-h", and the assimilative mode, denoted as "DEBOT-a". These changes has been documented in two peer-reviewed papers Einšpigel and Martinec (2015, 2017), hereinafter EM15 and EM16. The source code of DEBOT is freely available at `http://geo.mff.cuni.cz/~einspigel/debot.html`.

1 Shallow water equations

In modelling ocean circulation, the moving free surface represents a crucial problem. An approximate way to overcome this problem is by the so-called *shallow water approximation*. This approximation can be applied when the ver-

tical dimension of the solution domain is significantly smaller in comparison with the horizontal dimension. Under this assumption, the Navier–Stokes equations are reduced to the shallow water equations for the free-surface elevation and the horizontal components of flow velocity. The shallow water equations, which were first derived by Adhémar Jean Claude Barré de Saint–Venant, a french mechanician and mathematician, in 1871 (Barré de Saint-Venant, 1871), are used in the modelling of many geophysical phenomena, such as the oceans, atmosphere, shelf and coastal seas, rivers, and even avalanches. The equations can be derived from the incompressible Navier–Stokes system

$$\rho \left(\frac{\partial \vec{v}}{\partial t} + \nabla \cdot (\vec{v} \otimes \vec{v}) \right) = -\nabla p + \nabla \cdot \boldsymbol{\sigma} - 2\vec{\Omega} \times \vec{v} + \vec{g}, \tag{1}$$

where ρ is the applied density, $\vec{v}$ the velocity, $\vec{\Omega}$ the vector of the mean angular velocity of the Earth, $\boldsymbol{\sigma}$ a symmetric, trace-free deviatoric tensor and $\vec{g}$ is the vector of the gravitational acceleration. The system is supplemented with boundary conditions. In this thesis, we assume a friction vector at the bottom and that no fluid crosses the boundaries. The stress tensor $\boldsymbol{\sigma}$ is the *Reynolds tensor* which describes energy losses in large-scale ocean motions due to turbulences on very short scales. The derivation can be divided into three steps.

1. First, the so-called spherical approximation is applied. The radial distance of a material point in oceans is approximated by the mean Earth radius a.

2. The equations are expressed in a dimensionless form and terms of small magnitudes are neglected (the hydrostatic approximation).

3. The non-dimensionalized equations are integrated in the radial direction from the bottom to the surface, using the Leibniz integral rule and the appropriate boundary conditions are applied. Next, we assume the horizontal flow being only weakly dependent on depth such that the derivatives of velocities with respect to the radial direction are negligible.

The final form of the shallow water equations is

$$\frac{\partial \zeta}{\partial t} + \nabla_\Omega \cdot (h\vec{v}) = 0, \tag{2}$$

$$\frac{\partial (h\vec{v})}{\partial t} + \nabla_\Omega \cdot (h\vec{v} \otimes \vec{v}) = -gh\nabla_\Omega \zeta + fh\vec{v} \times \vec{e}_z - \vec{\tau}_{BF} + A_H \nabla_\Omega \cdot \boldsymbol{\sigma}, \tag{3}$$

where ζ is the surface elevation $\vec{v}$ horizontal, depth-averaged velocities, ∇_Ω is the spherical nabla operator, h the height of the water column from the ocean bottom to the surface, g is the gravitational constant, $f = 2\Omega \sin\phi$ is the Coriolis parameter, where Ω is the mean angular velocity of the Earth and ϕ the latitude, $\vec{\tau}_{BF}$ is the bottom-friction vector, A_H the eddy viscosity coefficient and $\boldsymbol{\sigma}$ the eddy viscosity tensor. The eddy viscosity term describes energy losses on large scales due to small-scale turbulences. The friction on the bottom of

the ocean is parametrized by a quadratic formula $\vec{\tau}_{BF} = r\vec{v}|\vec{v}|$ which is a standard way in ocean tide modelling (e.g., Egbert et al., 2004; Weis et al., 2008; Hill et al., 2011; Green and Nycander, 2013).

2 Numerical methods and tests

Let us briefly overview numerical methods used to solve the shallow water equations (2) and (3). The equations are approximated in space by finite differences on a staggered grid using the Arakawa C-grid (Arakawa and Lamb, 1977). The spatial resolution is defined by a user. The most of testing simulations whose results are discussed in Sections 3 and 4 are performed for the resolution of $15' \times 15'$. The model does not include the North pole area to avoid the pole singularity. Therefore, in this study, we consider an artificial continent at the North pole bounded by the 85° North parallel line. The time-stepping scheme in DEBOT is a generalized forward-backward scheme using a combination of a third-order Adams-Bashforth step with a fourth-order Adams-Moulton step (Shchepetkin and McWilliams, 2005, 2008). This is a stable and verified time-stepping scheme which computes values on the next time-level from three previous ones. The bottom friction is approximated by a semi-implicit scheme proposed by Backhaus (1983). The code of DEBOT is written in the free-form Fortran language with implemented C pre-processing switches and OpenMP parallelization.

Validity of the numerical methods are tested by the conservation of integral invariants. A set of tsunami experiments are performed on a globe with continents at the poles and an island at the equator. The bathymetry has a shape of a Gaussian hill which leads to the formation of a circle island at the equator. The initial elevation of the free surface is given by a Gaussian depression with the amplitude of 100 m. The initial velocities are set equal to zero and the bottom friction is omitted. We investigate the evolution of the total mass and total energy during the 10-day simulation for several settings of the turbulent viscosity coefficient A_H with the spatial resolutions $60' \times 60'$, $30' \times 30'$, $20' \times 20'$ and $15' \times 15'$. In all experiments, the total volume retains a constant value of -1.939×10^{14} m^3 with random deviations of the order m^3 which is of the order of the numerical errors. The evolution of the total energy is plotted in Figure 1. The testing of the energy demonstrates the validity of the numerical code since the energy is preserved in the case of zero eddy viscosity and decreases with non-zero viscosity. The decline of the energy is only slightly affected by the size of the spatial discretization step. The decline of the energy is greater with increasing eddy viscosity, however, the simulation becomes numerically unstable if the eddy viscosity is too large. This undesirable effect is probably an attribute of the time-stepping scheme in the case of too large A_H.

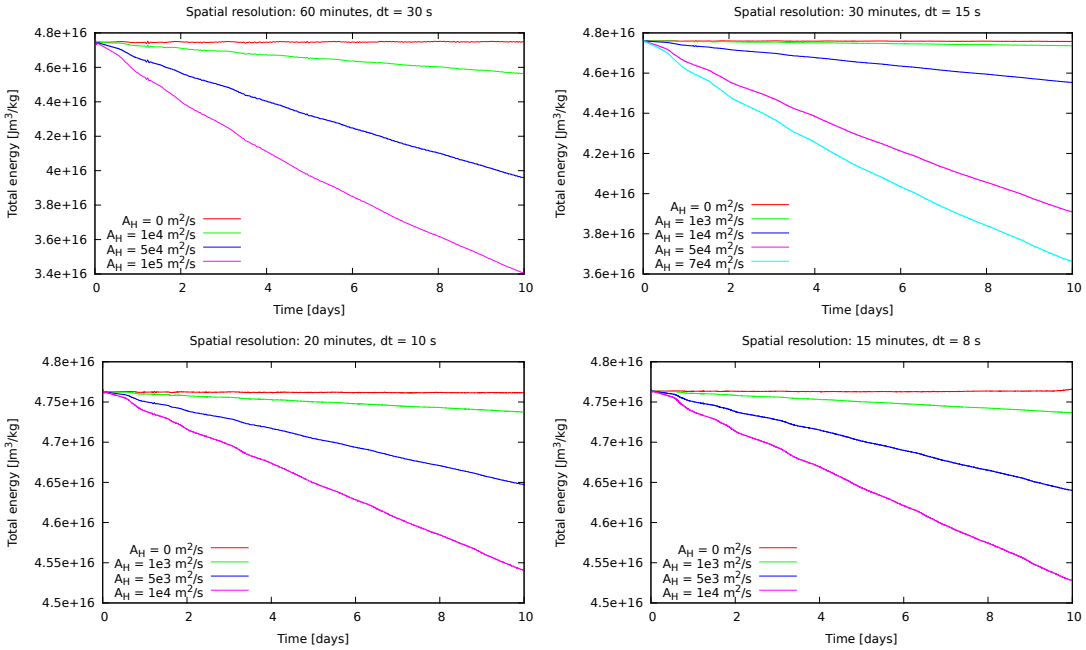

Figure 1: Evolution of the total energy from the tsunami experiment for spatial discretization of $60' \times 60'$, $30' \times 30'$, $20' \times 20'$ and $15' \times 15'$ and several values of the turbulent viscosity coefficient A_H.

3 DEBOT-h: a purely hydrodynamical model

3.1 Description of DEBOT

By purely hydrodynamical models we consider those tidal models whose solution is not constrained by any measurements of sea level, whether satellite altimetry or tide gauges data. Therefore, the model solution is given by equations of fluid motion, usually the shallow-water equation. DEBOT-h is such a model and this section is dedicated to it. DEBOT is based on the shallow water equations

$$\frac{\partial \zeta}{\partial t} + \nabla_\Omega \cdot (h\vec{v}) = 0, \tag{4}$$

$$\frac{\partial (h\vec{v})}{\partial t} + \nabla_\Omega \cdot (h\vec{v} \otimes \vec{v}) = -g_e h \nabla_\Omega \zeta + f h\vec{v} \times \vec{e}_z - \vec{\tau}_{BF} + A_H \nabla_\Omega \cdot \boldsymbol{\sigma} - \vec{\tau}_{ITD} + \vec{T}. \tag{5}$$

An attentive reader notices differences between equations (5) and (3) from the end of Section 1. First, the gravitational constant g is replaced by the "reduced gravity" g_e due to a parametrization of the self-attraction and loading of the water. Second, the internal tide drag $\vec{\tau}_{ITD}$, an additional dissipative term, is added. Third, equation (5) contains the tidal forcing $\vec{T}$.

The self-attraction and loading (SAL) of the water is an essential part of ocean tide modelling since its omission can change computed tidal amplitudes by 10 % or more and phases by 30° or more (Ray, 1998). The effect of SAL can be included as an additional forcing $gh\nabla_\Omega \zeta_{\mathrm{SAL}}$ where ζ_{SAL} is the equilibrium-

like tide. A simple scalar approximation of the SAL, proposed by Accad and Pekeris (1978), is adopted in DEBOT

$$\zeta_{\mathrm{SAL}} = \epsilon\zeta, \tag{6}$$

where ϵ is the scalar factor or SAL coefficient. This eventually leads to a replacement of the gravitational constant g by the "reduced gravity" $g_\epsilon = (1-\epsilon)g$ in equation (5).

Energy conversion of barotropic tidal currents into baroclinic (internal) waves is accounted for by the internal tide drag (ITD) which is formulated as the vector

$$\vec{\tau}_{ITD} = \kappa\frac{\pi}{L}\hat{h}^2 N_b, \tag{7}$$

where $\hat{h}$ is the bottom roughness, which is estimated by a standard deviation of bathymetric data, N_b is the observed buoyancy frequency at the seabed and L is a wave or topography length scale which is a tunable parameter. In this study, for practical reasons, we keep $L = 10\,000$ m as suggested by Jayne and St. Laurent (2001); Green and Nycander (2013) and introduce an independent tunable factor κ which is of the order $\mathcal{O}(1)$.

The tidal forcing $\vec{T}$ is generated by the full lunisolar tidal potential of the second and third degree V_2 and V_3, respectively (e.g., Doodson, 1921; Melchior, 1983; Smith, 1999; Fok, 2012)

$$\begin{aligned} V_2 = \frac{3}{4}\frac{GMa^2}{d^3}\Big[&\cos^2\phi\cos^2\delta\cos(2\tau) + \\ &\sin(2\phi)\sin(2\delta)\cos\tau + \\ &3\left(\sin^2\phi - \frac{1}{3}\right)\left(\sin^2\delta - \frac{1}{3}\right)\Big], \end{aligned} \tag{8}$$

$$\begin{aligned} V_3 = \frac{1}{4}\frac{GMa^3}{d^4}\Big[&\left(5\sin^2\phi - 3\right)\left(5\sin^2\delta - 3\right)\sin\phi\sin\delta + \\ &\frac{3}{2}\left(5\sin^2\phi - 1\right)\left(5\sin^2\delta - 1\right)\cos\phi\cos\delta\cos\tau + \\ &\frac{15}{4}\sin(2\phi)\cos\phi\sin(2\delta)\cos\delta\cos(2\tau) + \\ &\frac{5}{2}\cos^3\phi\cos^3\delta\cos(3\tau)\Big], \end{aligned} \tag{9}$$

where G is the gravitational constant, M the mass of a celestial body, d and δ are the geocentric distance and the declination of the celestial body, respectively and τ the local hour angle, which is related to the right ascension α by

$$\tau = \Omega T_{Gr} + \lambda - \alpha, \tag{10}$$

where T_{Gr} is the Greenwich sidereal time and λ is the longitude.

Table 1: The M_2 RMS differences (in cm) of DEBOT-h and other purely hydrodynamical models against the deep ocean and shelf seas tidal stations (RMS_{TS}) and against TPXO8 (RMS_{alt}).

	Deep ocean		Shelf seas	
Model	RMS_{TS}	RMS_{alt}	RMS_{TS}	RMS_{alt}
DEBOT-h	**9.92**	**10.38**	**31.3**	**22.5**
HIM	8.75	5.25	33.7	22.3
OTIS-GN	7.54	6.76	25.3	18.6
STORMTIDE	8.33	7.76	48.2	27.9
OTIS	5.63	4.65	23.6	24.0
STM-1B	12.69	7.74	30.5	25.8
HYCOM	7.82	7.00	49.0	26.2

3.2 Results of simulations

The DEBOT-h solution is dependant on several parameters: the ITD factor κ, SAL coefficient ϵ, eddy viscosity coefficient A_H, bottom friction coefficient c_{BF}, bathymetric dataset and spatial resolution. Hundreds of DEBOT-h simulations have been carried out and compared to "ground truth" data from deep-ocean bottom pressure recorders, shelf seas tidal stations and tide gauges along coastlines. Statistical methods are used to assess the accuracy of DEBOT: root mean squares (RMS) differences, root sum squares (RSS), median absolute differences (MAD) and absolute vector differences (AVD).

After performing hundreds of simulations, we concluded that the best DEBOT-h setting in terms of the RMS statistic is as follows: the GEBCO bathymetry, $\kappa = 1.4$, $\epsilon = 0.1$, $A_H = 10^4 \frac{\mathrm{m}^2}{\mathrm{s}}$ and $c_{BF} = 0.003$. This setting is picked up as a compromise between the deep ocean and shelf seas. Table 1 shows the M_2 RMS differences of this model setting against the testing tidal stations (RMS_{TS}) and also against TPXO8, an independent data-assimilative model, over the entire ocean domain (RMS_{alt}). The RMS differences of state-of-the-art purely hydrodynamical models are also shown for references. The other models are HIM (Arbic et al., 2008), OTIS-GN (Green and Nycander, 2013), STORMTIDE (Müller et al., 2012), OTIS (Egbert et al., 2004), STM-1B (Hill et al., 2011) and HYCOM (Arbic et al., 2010). The RMS values are taken from Stammer et al. (2014). We can say that DEBOT-h is comparable in accuracy with the other models in the shelf seas, however it is still a little bit worse in the deep ocean. This may be caused by several reasons. First, different bathymetry and resolution of the other models (DEBOT-h has the resolution of $15'$ while the others $7.5'$ or finer). However, since the RMS differences of DEBOT-h on the continental shelves are relatively good, we rather think that the problem may be in the parameterization of the ITD and the scalar approximation of the SAL. Future works should be focused on an implementation of more rigorous parameterization of the ITD and SAL.

Besides statistical methods, model errors might be also evaluated by a vi-

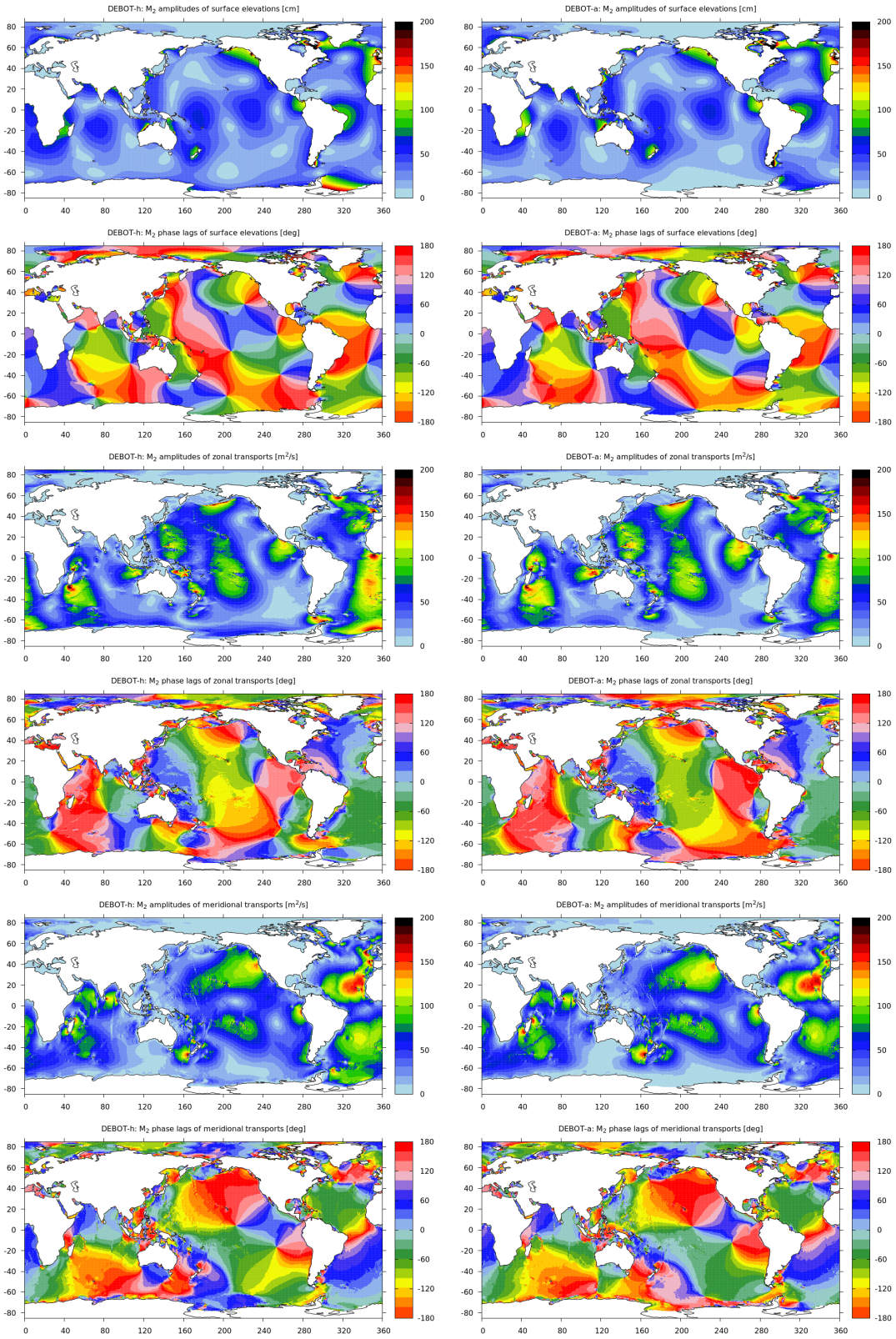

Figure 2: Comparison of DEBOT-h (left) and DEBOT-a (right): M_2 amplitudes and Greenwich phase lags of the surface elevations (two top panels), zonal transports (two middle panels) and meridional transports (two bottom panels).

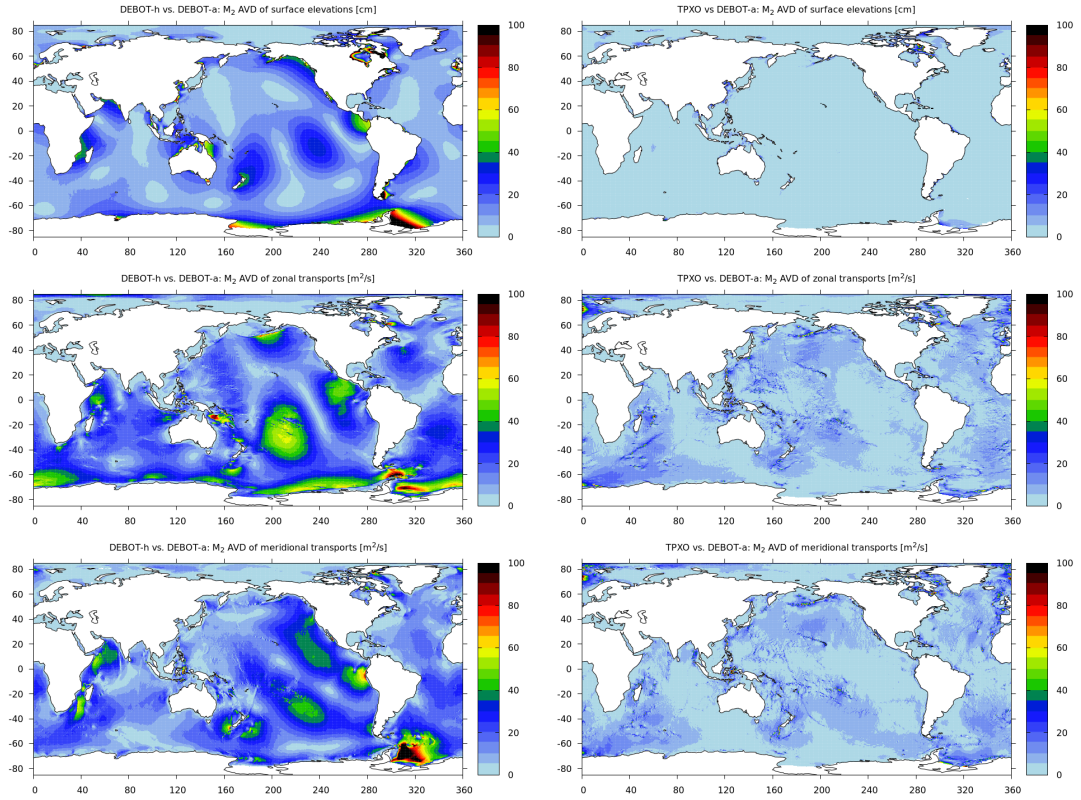

Figure 3: Absolute vector differences between DEBOT-h and DEBOT-a (left) and DEBOT-a and TPXO (right) for the M_2 surface elevations (top), zonal transports (middle) and meridional transports (bottom).

sual inspection of global charts. Figure 2 shows the M_2 amplitudes and Greenwich phase lags of the surface elevations and zonal and meridional transports ($h\vec{v}$) for DEBOT-h and DEBOT-a (Section 4). Moreover, Figure 3 shows the absolute vector differences of all three variables between DEBOT-h and DEBOT-a and also between DEBOT-a and TPXO8 for reference. As can be seen, general patterns of both DEBOT-h and DEBOT-a are same, however there are some problematic spots. Especially two large areas in the Pacific ocean with the surface elevations AVD up to 40 cm which are probably the main reason of large $\mathrm{RMS}_{\mathrm{alt}}$ in the deep ocean. Another problematic areas are a belt along the west coast of North America and the Southern Ocean, especially in the Weddel and Ross seas which are mostly covered by ice shelves. The ice-covered area of the Weddel and Ross seas are not included in our solution and obviously, their omission produces large errors. On the other hand, DEBOT-h seems to be generally good in the Atlantic and Indian oceans and the northwest part of the Pacific ocean (except some smaller areas, e.g., Hudson bay, the Mozambique channel, the Patagonian shelf, the Irish sea, etc.).

4 DEBOT-a: an assimilative model

In this section, our attention is focused on the assimilative version of the DEBOT model — DEBOT-a. DEBOT-a is constructed as an extension of DEBOT-h, which means that it is also a non-linear, time-domain model with the full lunisolar tidal forcing. This is an alternative model compared to the state-of-the-art assimilative models TPXO (Egbert et al., 1994; Egbert and Erofeeva, 2002), FES (Lyard et al., 2006; Carrère et al., 2012) or HAMTIDE (Zahel, 1995; Taguchi et al., 2014) which are all based on linearised, spectral-domain momentum and continuity equations and a general inversion scheme is applied for the assimilation of satellite altimetry data.

4.1 The assimilation scheme

The assimilation scheme used in DEBOT-a is based on a periodical "upgrade" of the surface elevation. It means that the model solution is given by the hydrodynamical model and at regular intervals ΔT, an assimilation process is applied and the model solution is constrained by data information. As data constraints, we use the DTU10 model (Cheng and Andersen, 2012) which is a freely available, state-of-the-art empirical model comparable in accuracy to other empirical models such as GOT4.8 (Ray, 1999, 2013), EOT11a (Savcenko and Bosch, 2012), OSU12 (Fok, 2012) or the assimilative models mentioned above, see Stammer et al. (2014) for their intercomparison. DTU10 provides the surface elevation amplitudes and Greenwich phase lags of 9 tidal constituents (Q_1, O_1, P_1, K_1, N_2, M_2, S_2, K_2 and M_4) on a $7.5'$ grid. Signals of other tidal constituents are given by the hydrodynamical solution only and are not constrained by any data. The assimilation process is a weighted summation of the surface elevations given by the hydrodynamical model, ζ_D, and the data, ζ_E, $\zeta = w\zeta_E + (1-w)\zeta_D$, where $w \in (0,1)$ is the weight given to the data and ζ the "upgraded" surface elevation.

The assimilation process is dependent on two parameters, the assimilation interval ΔT and the weight w. These parameters are examined through series of tests against the tidal stations. Figures 4 and 5 show the relative RMS differences between DEBOT-a and the testing data for various values of ΔT and w, respectively. The assimilation process has a great impact on resulted elevations even for relatively large intervals $\Delta T = 1-2$ h and relatively small weights $w < 0.5$. However, better RMS differences are generally achieved with smaller intervals and larger weights.

4.2 Results of realistic simulations

We compare our results with other state-of-the-art empirical and assimilative models for the eight major tidal constituents which is summarized in Tables 2, 3 and 4. The empirical models are DTU10, GOT4.8, OSU12 and EOT11a. The assimilative models are HAMTIDE, FES2012 and TPXO8. The appropriate values are taken from Stammer et al. (2014). For the comparison we use the results

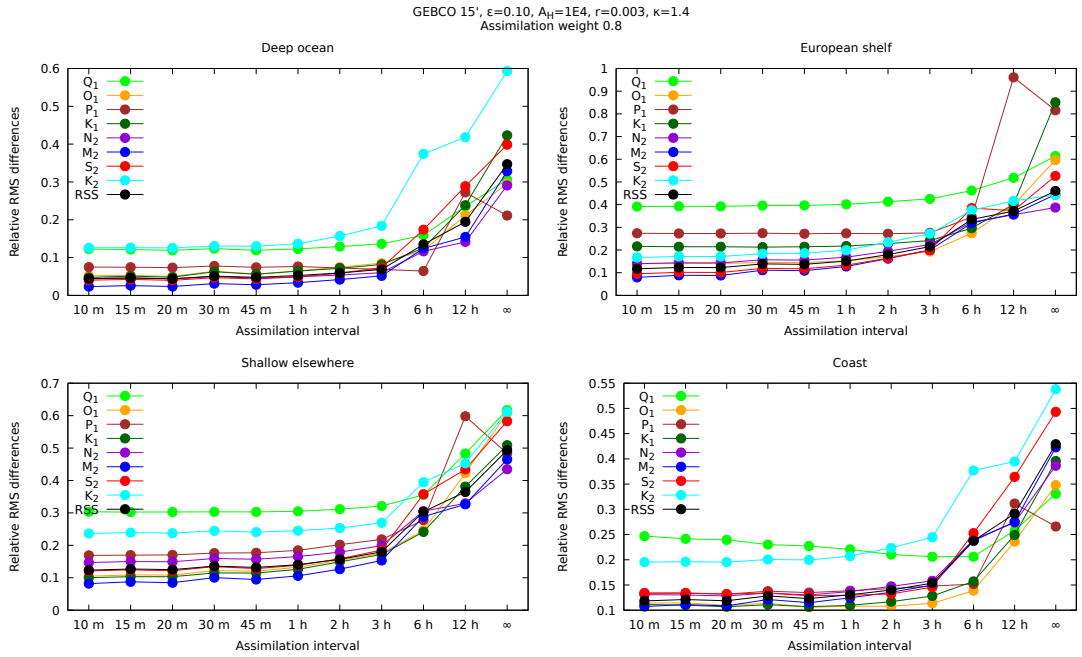

Figure 4: The relative RMS differences between DEBOT-a and the tidal stations for various values of the assimilation interval ΔT. Note that ∞ denotes results of non-assimilative DEBOT-h.

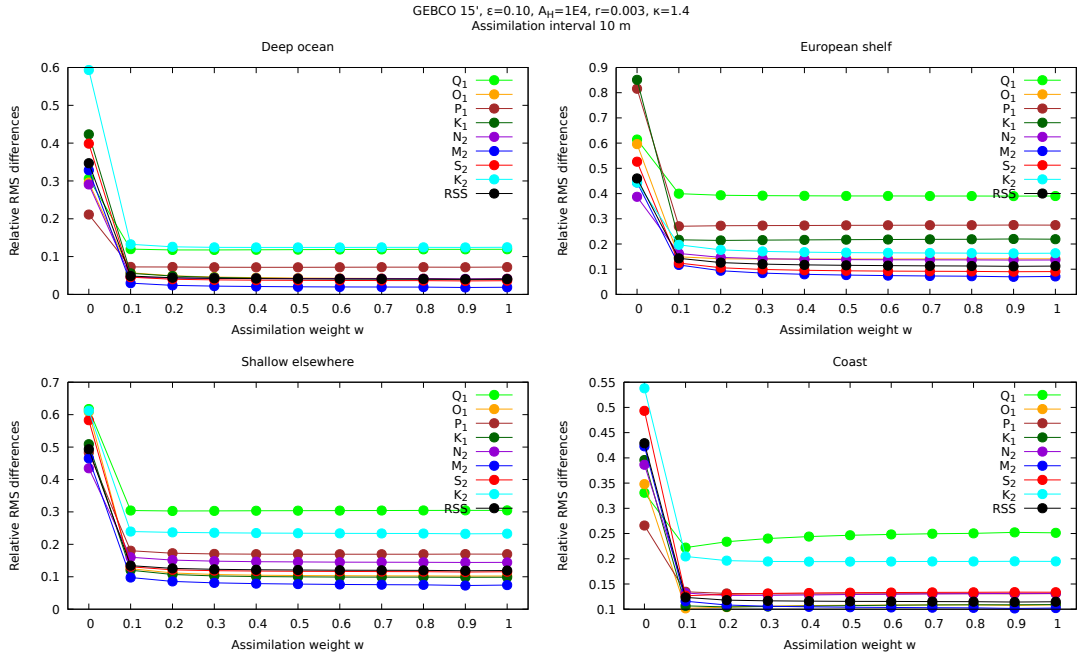

Figure 5: The relative RMS differences between DEBOT-a and the tidal stations for various values of the assimilation weight w. Note that 0 denotes results of non-assimilative DEBOT-h.

of the simulation with $\Delta T = 10$ min and $w = 1.0$. In these tables, the RSS are computed from the RMS values of the eight major tides only.

In the deep ocean (Table 2), DEBOT-a is quite comparable to the other models although some improvements are still required as O_1, K_1 and K_2 are a little bit worse than other models. This may be caused by errors of the prior hydrodynamical model and we believe that better accuracy of DEBOT-a can be achieved by future improvements of hydrodynamical DEBOT-h.

It is interesting that on the northwest European shelf (Table 3), DEBOT-a is very good for diurnal constituents, approaching the best numbers, but relatively poor for semi-diurnal constituents, especially for the M_2 tide where DEBOT-a drops behind the other model by about 0.5–3 cm. This suggest that the RMS statistic of the European shelf datasets, which consists of only 76 tidal stations, is affected by some outliers. For the NW European shelf, the median of the M_2 AVD is 2.85 cm but the mean value is 5.56 cm. Hence, while the M_2 model errors are less than 3 cm at most locations on the NW European shelf, there are still some problematic spots with much larger errors, namely the station on Jersey island in the English channel and some stations in the Irish sea close to a land. On the other hand, the RMS statistic of the other shelf seas seems to be less affected by outliers and more reliable. The median of the M_2 AVD is 2.22 cm in these shelf seas and the mean value is 3.92 cm. The RMS differences of DEBOT-a in the "shelf seas elsewhere" are comparable to other models results without extremal values, as you can see in Table 3.

Finally, DEBOT-a is also comparable with the other models along continental coastlines, see Table 4. Some tidal station locations are deemed by DEBOT to be land and these stations are not included in the RMS and MAD statistics. This is a little inconsistent with the RMS and median values from other models which were computed from all coastal stations using some extrapolation where it was necessary (Stammer et al., 2014). Hence, the median statistic is probably more meaningful than the RMS in this case. Nevertheless, the DEBOT-a results are good when compared to the other models, regardless of the used method.

5 Modelling of minor tidal constituents

So far, our attention has been focused on the eight major tides only. However, as DEBOT is a non-linear ocean model forced by the full lunisolar potential of the second and third degree, it allows us to model all tidal constituents simultaneously including non-linear compound tides. Although signals of minor constituents are generally very small compared to the major constituents (especially to M_2), reaching amplitudes usually several millimeters in the deep ocean and several centimeters in the shallow shelf seas, knowledge of them might still be useful in some applications. We should note that long-term tides of greater periods than diurnal (e.g., fortnightly Mf, monthly Mm, semi-annual Ssa, etc.) are not addressed here due to lack of high-quality testing data. Minor tidal constituents are usually not included in global ocean mod-

Table 2: Tidal signals and RMS differences of DEBOT-a and state-of-the-art empirical and assimilative models against the deep ocean BPR stations (in cm).

	Q_1	O_1	P_1	K_1	N_2	M_2	S_2	K_2	RSS
Signal	1.79	8.75	3.99	12.51	6.36	30.22	11.21	3.12	36.62
DEBOT-a	**0.214**	**0.363**	**0.288**	**0.498**	**0.264**	**0.573**	**0.406**	**0.389**	**1.106**
DTU10	0.226	0.277	0.292	0.449	0.274	0.613	0.415	0.383	1.088
GOT4.8	0.165	0.296	0.234	0.423	0.252	0.510	0.369	0.209	0.923
OSU12	0.304	0.369	0.194	0.430	0.441	0.578	0.940	0.287	1.395
EOT11a	0.232	0.317	0.224	0.404	0.335	0.564	0.428	0.365	1.056
HAMTIDE	0.160	0.317	0.199	0.373	0.245	0.513	0.397	0.176	0.904
FES2012	0.216	0.309	0.355	0.471	0.342	0.658	0.407	0.223	1.120
TPXO8	0.153	0.310	0.181	0.442	0.201	0.523	0.338	0.151	0.894

Table 3: Tidal signals and RMS differences of DEBOT-a and state-of-the-art empirical and assimilative models against the shelf seas tidal stations (in cm).

	Q_1	O_1	P_1	K_1	N_2	M_2	S_2	K_2	RSS
NW European shelf									
Signal	2.1	5.6	1.5	5.5	17.0	87.7	30.0	7.3	94.9
DEBOT-a	**0.84**	**0.79**	**0.41**	**1.21**	**2.32**	**6.25**	**2.72**	**1.19**	**7.50**
DTU10	0.83	0.81	0.51	1.27	2.17	3.50	2.38	0.92	5.17
GOT4.8	0.93	0.92	0.55	1.30	1.97	5.87	2.51	1.09	7.04
OSU12	1.11	1.24	0.69	1.53	1.77	5.04	4.04	1.29	7.22
EOT11a	0.85	0.83	0.50	1.24	2.13	5.53	3.43	1.13	7.17
HAMTIDE	0.92	1.96	0.47	1.14	1.65	3.11	2.64	0.92	5.14
FES2012	0.88	0.82	0.71	1.19	1.39	3.71	1.94	0.63	4.82
TPXO8	0.88	0.72	0.46	1.21	1.58	3.85	1.70	0.74	4.87
Shelf seas elsewhere									
Signal	2.7	10.9	5.9	17.1	12.5	54.0	21.7	7.1	63.6
DEBOT-a	**0.82**	**1.12**	**1.00**	**1.68**	**1.81**	**4.01**	**2.51**	**1.65**	**5.84**
DTU10	0.82	1.11	1.06	1.70	1.80	3.44	2.39	1.57	5.40
GOT4.8	0.69	1.05	0.92	1.68	1.97	4.14	2.93	1.59	6.11
OSU12	1.00	1.17	0.84	1.75	1.87	4.61	3.00	1.15	6.42
EOT11a	0.73	1.07	0.78	1.64	1.86	5.05	3.39	1.31	6.87
HAMTIDE	0.97	1.16	0.80	2.02	2.01	3.89	2.52	1.44	5.88
FES2012	0.80	1.00	0.89	1.51	1.58	3.33	2.30	1.02	4.96
TPXO8	0.82	1.00	0.82	1.47	2.00	3.50	1.93	1.12	5.07

Table 4: Tidal signals, RMS differences and median absolute differences of DEBOT-a and state-of-the-art empirical and assimilative models against the coastal tide gauges (in cm).

	Q_1	O_1	P_1	K_1	N_2	M_2	S_2	K_2	RSS
Signal	1.9	9.7	4.9	15.9	11.2	55.5	21.4	6.0	63.8
RMS differences									
DEBOT-a	**0.49**	**1.06**	**0.65**	**1.74**	**1.47**	**5.68**	**2.87**	**1.17**	**6.99**
DTU10	0.62	1.29	0.73	2.08	1.72	5.24	2.68	1.40	6.82
GOT4.8	0.46	1.01	0.57	1.80	1.92	7.00	3.53	1.34	8.47
OSU12	1.14	1.68	1.20	3.20	2.15	9.01	5.31	1.41	11.48
EOT11a	0.54	1.32	0.85	2.38	1.78	4.50	2.84	1.49	6.49
HAMTIDE	0.29	1.42	0.71	2.65	2.27	14.63	5.41	1.80	16.17
FES2012	0.32	0.89	0.61	1.65	1.74	6.60	2.27	0.77	7.50
TPXO8	0.43	1.13	0.93	2.01	3.34	15.65	7.79	2.12	18.10
Median absolute differences									
DEBOT-a	**0.16**	**0.34**	**0.28**	**0.56**	**0.37**	**1.20**	**0.64**	**0.40**	**1.64**
DTU10	0.21	0.37	0.37	0.67	0.42	1.28	0.77	0.42	1.83
GOT4.8	0.14	0.42	0.27	0.62	0.60	1.30	0.80	0.37	1.87
OSU12	0.35	0.46	0.26	0.62	0.59	1.19	1.58	0.34	2.27
EOT11a	0.18	0.36	0.30	0.61	0.41	1.06	0.65	0.32	1.56
HAMTIDE	0.12	0.46	0.27	0.68	0.40	1.02	0.66	0.28	1.57
FES2012	0.18	0.43	0.44	0.66	0.47	1.36	0.66	0.24	1.85
TPXO8	0.13	0.26	0.25	0.58	0.28	1.49	0.49	0.21	1.75

els except for M_4 which is a part of six of the seven modern empirical and assimilative models mentioned in the previous chapter (HAMTIDE is the exception). TPXO8 includes also the non-linear MN_4 and MS_4 tides, however only FES2012 provides global atlases of larger number of tidal constituents, 33 tides in total.

Analogously to the previous chapters, we compute the RMS differences and MAD for selected minor tidal constituents. The constituents was chosen so that DEBOT can be compared to other models. Final results are summarized in Tables 5 (deep ocean) and 6 (shelf seas) and graphically in Figure 6. DEBOT-a is compared to FES2012, TPXO8 (for three compound tides) and in the deep ocean also to GOT4.8 whose values were inferred from the tidal admittance (Ray, 2013). In Figure 6, we also plot values from DEBOT-h to show that the assimilation process does not affect minor tides. Of course, this is not a case of M_4 which is constrained by the DTU10 dataset.

The values inferred from GOT4.8 in the deep ocean are generally better than the DEBOT-a ones except for $2N_2$ and μ_2. This suggests that it could be beneficial for DEBOT-a—at least in the deep ocean—to be constrained by another data of harmonic constants of minor diurnal and semi-diurnal tides deduced from an empirical model using the tidal admittance. The results

Table 5: Selected minor tidal constituents, their tidal signals and RMS differences between the deep ocean BPR stations and the ocean models (in cm).

		RMS differences			
	Signal	**DEBOT-a**	GOT4.8	FES2012	TPXO8
$2Q_1$	0.25	**0.093**	0.085		
J_1	0.71	**0.344**	0.178	0.131	
OO_1	0.43	**0.376**	0.265		
$2N_2$	0.80	**0.226**	0.271	0.119	
μ_2	0.95	**0.229**	0.409	0.197	
ν_2	1.13	**0.375**	0.075	0.129	
L_2	0.75	**0.393**	0.250	0.235	
T_2	0.63	**0.294**	0.130	0.194	
R_2	0.12	**0.102**		0.101	
M_3	0.23	**0.096**		0.231	
MN_4	0.09	**0.082**		0.073	0.068
M_4	0.22	**0.092**	0.089	0.115	0.075
MS_4	0.12	**0.113**		0.104	0.134

of FES2012 are generally better than DEBOT-a for diurnal and semi-diurnal tides but DEBOT-a is obviously better for third-diurnal M_3 owing to the implemented forcing term of the third degree. Regarding non-linear MN_4, M_4 and MS_4, the results of all three models, DEBOT-a, FES2012 and TPXO8, seem to be roughly equal except for the NW European shelf where TPXO8 predictions are significantly better, probably due to a very high resolution of $2'$ for shelf areas. As mentioned, M_4 is included also in DTU10, EOT11a and OSU12. Their RMS differences and MAD against the tidal stations are not shown here but they are roughly the same as in the case of DEBOT-a.

In the deep ocean, the relative RMS differences for minor diurnal and semi-diurnal tides are about 10–30 % of the signal (except for very small R_2) which is the same as for the eight major tides. This suggests that possible future improvements of DEBOT-h discussed in Section 3 (finer resolution, more rigorous treatment of the ITD and SAL) should also lead to more precise determination of minor tidal constituents. In the shelf seas, the relative differences of minor tides are much larger, however, we should emphasize that the RMS differences and MAD for the minor tides in the shelf seas are computed from relatively small number of stations and thus they can not provide a general description of a global model and are rather indicative.

Conclusions

The DEBOT model, a time-domain global barotropic ocean model has been developed and is presented. DEBOT is primarily designed for ocean flow generated by the tidal attraction of the Moon and the Sun, however, it can be used

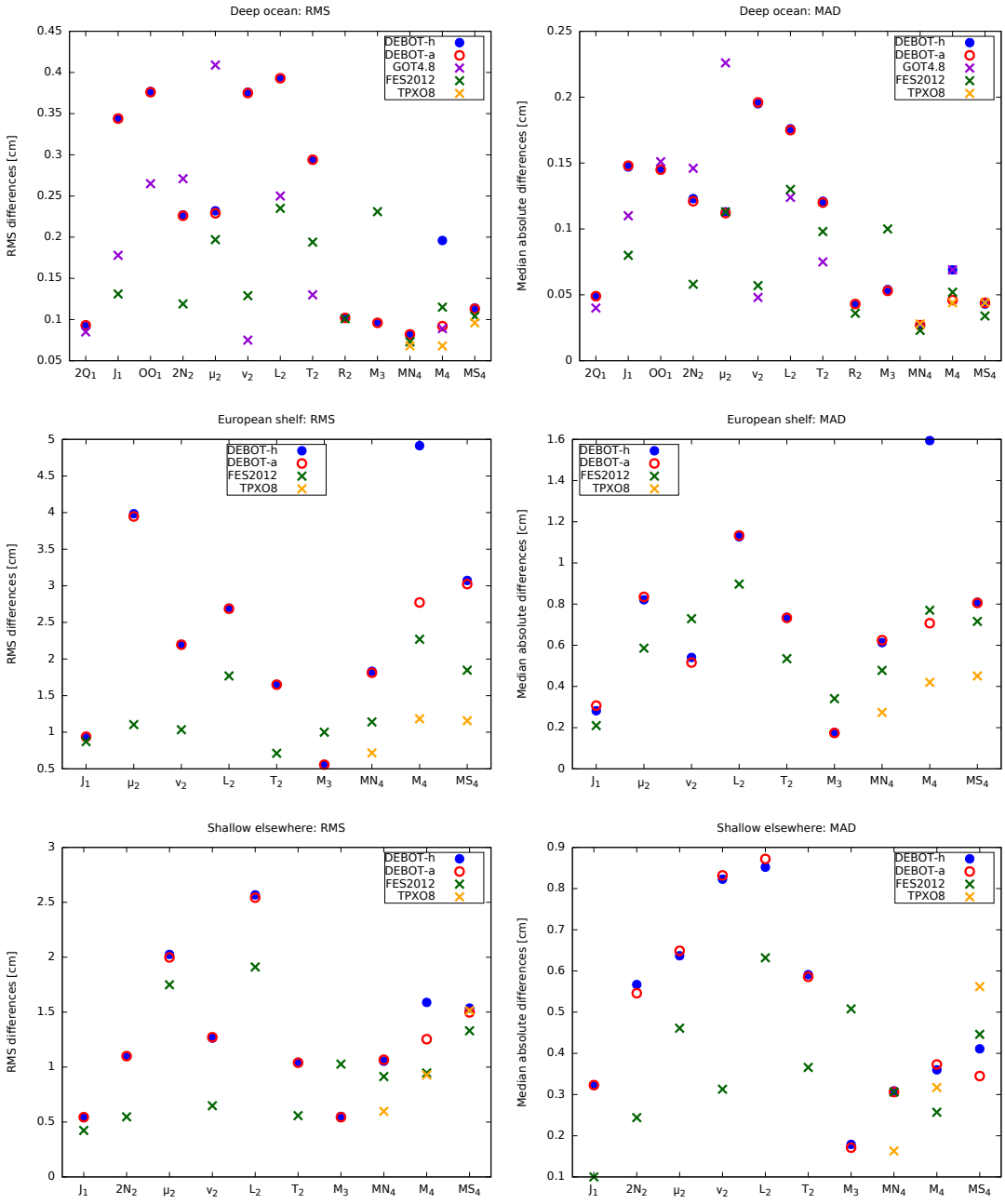

Figure 6: The RMS differences (left) and median absolute differences (right) between the ocean models and the deep ocean (top) and shelf seas (middle and bottom) tidal stations for selected minor tidal constituents.

Table 6: Selected minor tidal constituents, their tidal signals, RMS differences and median absolute differences between the shelf seas tidal stations and ocean models (in cm).

		RMS differences			*Median absolute differences*		
	Signal	**DEBOT-a**	FES2012	TPXO8	**DEBOT-a**	FES2012	TPXO8
			NW European shelf				
J_1	0.92	**0.938**	0.872		**0.307**	0.210	
μ_2	4.44	**3.947**	1.104		**0.835**	0.586	
ν_2	3.24	**2.195**	1.034		**0.516**	0.729	
L_2	4.57	**2.686**	1.769		**1.133**	0.897	
T_2	1.99	**1.650**	0.712		**0.733**	0.535	
M_3	0.92	**0.557**	1.000		**0.174**	0.341	
MN_4	1.76	**1.812**	1.141	0.717	**0.625**	0.478	0.274
M_4	4.68	**2.772**	2.270	1.183	**0.707**	0.770	0.420
MS_4	2.91	**3.024**	1.847	1.157	**0.806**	0.716	0.451
			Shelf seas elsewhere				
J_1	0.85	**0.544**	0.423		**0.323**	0.100	
$2N_2$	1.70	**1.100**	0.547		**0.546**	0.244	
μ_2	2.44	**1.998**	1.749		**0.649**	0.461	
ν_2	2.18	**1.272**	0.648		**0.832**	0.313	
L_2	3.13	**2.543**	1.911		**0.872**	0.632	
T_2	1.69	**1.040**	0.558		**0.586**	0.366	
M_3	1.18	**0.544**	1.027		**0.171**	0.508	
MN_4	1.45	**1.067**	0.914	0.597	**0.306**	0.306	0.163
M_4	1.82	**1.254**	0.946	0.928	**0.373**	0.257	0.317
MS_4	1.49	**1.498**	1.331	1.515	**0.345**	0.446	0.562

for other ocean applications where the shallow water approximation is convenient, for instance, tsunami wave propagation.

In Section 1, the derivation of the shallow water equations from the complete Navier-Stokes equations is generally described. The shallow water equations are a base for the numerical model (Section 2). The experiments, which comprise a tsunami wave propagating through the global ocean with an artificial island, has tested the conservation of the total mass and the total energy of the numerical model. The results of the tests are satisfactory, meaning that the total mass is preserved in all experiments and the total energy is preserved in the case of zero eddy viscosity and decreases with a non-zero viscosity (Figure 1). The eddy viscosity can effectively attenuate the energy, however, a too large eddy viscosity coefficient makes the computations unstable and results in an obviously unnatural increase in the energy.

As mentioned, DEBOT is designed for precise global ocean tides simulations. The model can be launched in two modes: the purely hydrodynamical mode, DEBOT-h, and assimilative mode, DEBOT-a.

Purely hydrodynamical DEBOT-h is presented in Section 3. DEBOT-h predictions are tested against the datasets of the deep ocean BPR stations, shelf seas tidal station and tide gauges along continental coastlines. A parametric study has been performed to investigate effects of input parameters and to find the best setting. DEBOT-h is comparable in accuracy with the state-of-the-art purely hydrodynamical models (Table 1) in the shelf seas however it is a bit worse in the deep ocean which may be caused by a coarser resolution, the scalar approximation of the SAL or the parameterization of the ITD. A more rigorous treatment of the ITD and SAL and their possible implementation in DEBOT will be addressed in future works in order to reach generally better accuracy. We also compares DEBOT-h with its data-assimilative version, DEBOT-a to find possible problematic areas of purely hydrodynamical modelling (Figures 2 and 3). Larger errors are produced in the Southern ocean which is caused by the omission of the ice-covered Weddel and Ross seas from the DEBOT model domain. These seas should be definitively included in future version of DEBOT.

DEBOT-a, the assimilative version of DEBOT, is introduced in Section 4. The author proposes a simply yet efficient assimilation scheme which can be used in a time-domain model and it is an alternative to spectral-domain general inversion schemes used in FES, TPXO and HAMTIDE. The surface elevation are periodically constrained by the elevations of the empirical model DTU10. The tests against the "ground truth" tidal data prove that DEBOT-a is comparable in accuracy with the state-of-the-art empirical and assimilative ocean tide models though there are still some locations where DEBOT-a does not reach desired accuracy, e.g., for semi-diurnal tides on the northwest European shelf. We believe that future improvements of prior hydrodynamical model (DEBOT-h) will allow us to achieve better results with DEBOT-a, also in the problematic locations.

Finally, minor tidal constituents and their model predictions are discussed in Chapter 5. As DEBOT is a non-linear model with the full lunisolar forcing, all tidal constituents can be modelled simultaneously. Selected minor tides modelled by DEBOT-a are tested against the tidal stations and compared with FES2012, TPXO8 and minor tides inferred from GOT4.8. Three conclusions can be drawn: (1) Good results for M_3 (in comparison with FES2012). (2) Roughly equal predictions of the non-linear compound MN_4, M_4 and MS_4 tides as FES and TPXO8, except for the NW European shelf where TPXO8 is better. (3) Generally worse predictions of diurnal and semi-diurnal minor tides than FES and GOT4.8. These tides are not constrained by data and are given by the purely hydrodynamical solution. The future improvements of DEBOT-h, discussed above, should lead to a better estimation of the minor tides too.

DEBOT can be useful for those applications where other ocean tide models are not suitable. The primary goal and original motivation was to use DEBOT for the research conducted in related geophysical disciplines. The model has already been used to study the magnetic field induced by ocean tides (Velímský et al., 2016) and the influence of ocean tides on the Earth's rotation

(Schindelegger et al., 2016). The source code of DEBOT is freely available at `http://geo.mff.cuni.cz/~einspigel/debot.html`.

Bibliography

Y. Accad and C. L. Pekeris. Solution of the tidal equations for the M_2 and S_2 tides in the world oceans from a knowledge of the tidal potential alone. *Phil. Trans. R. Soc. A*, 290(1368):235–266, 1978.

A. Arakawa and V. L. Lamb. Computational design of the basic dynamical processes of the UCLA general circulation model. In J. Chang, editor, *Methods in Computational Physics, Vol. 17*, pages 174–265. Academic Press, 1977.

B. K. Arbic, J. X. Mitrovica, D. R. MacAyeal, and G. A. Milne. On the factors behind large Labrador Sea tides during the last glacial cycle and the potential implications for Heinrich events. *Paleoceanography*, 23:PA3211, 2008. doi: 10.1029/2007PA001573.

B. K. Arbic, A. J. Wallcraft, and E. J. Metzger. Concurrent simulation of the eddying general circulation and tides in a global ocean model. *Ocean Model.*, 32:175–187, 2010.

J. O. Backhaus. A semi-implicit scheme for the shallow water equations for application to shelf sea modeling. *Cont. Sh. Res*, 2(4):243–254, 1983.

A. J. C. Barré de Saint-Venant. Théorie du mouvement non-permanent des eaux, avec application aux crues des rivières et à l'introduction des marées dans leur lit. *C. R. Acad. Sc. Paris*, 73:147–153, 1871.

L. Carrère, F. Lyard, M. Cancet, A. Guillot, and L. Roblou. FES 2012: A new global tidal model taking advantage of nearly 20 years of altimetry. Paper presented at The Symposium 20 Years of Progress in Radar Altimetry, Venice, 2012.

Y. Cheng and O. B. Andersen. Multimission empirical ocean tide modeling for shallow waters and polar seas. *J. Geophys. Res.*, 116(C11001):540–552, 2012.

A. T. Doodson. The harmonic development of the tide-generating potential. *Proc. R. Soc. A*, 100(704):305–329, 1921.

G. D. Egbert and S. Y. Erofeeva. Efficient inverse modeling of barotropic ocean tides. *J. Atmos. Oceanic Tech.*, 19:183–204, 2002.

G. D. Egbert, A. F. Bennett, and M. G. G. Foreman. TOPEX/Poseidon tides estimated using a global inverse model. *J. Geophys. Res.*, 99:24821–24852, 1994.

G. D. Egbert, R. D. Ray, and B. G. Bills. Numerical modeling of the global semidiurnal tide in the present day and in the last glacial maximum. *J. Geophys. Res.*, 109 (C03003), 2004. doi: 10.1029/2003JC001973.

D. Einšpigel. Barotropic ocean tide model. Master's thesis, Charles University in Prague, Prague, May 2012.

D. Einšpigel and L. Eisner. The differences in the detectability of perforation shots and microseismic events in the surface monitoring: the attenuation effect. *Acta Geodyn. Geomater.*, 11(2):159–164, 2014. doi: 10.13168/AGG.2013.0062.

D. Einšpigel and Z. Martinec. A new derivation of the shallow water equations in geographical coordinates and their application to the global barotropic ocean model (the DEBOT model). *Ocean Modelling*, 92:85–100, 2015. doi: 10.1016/j.ocemod.2015.05.006.

D. Einšpigel and Z. Martinec. Time-domain modelling of global ocean tides generated by the full lunisolar potential. *Ocean Dyn.*, 67(2):165–189, 2017. doi: 10.1007/s10236-016-1016-1.

H. S. Fok. *Ocean tides modeling using satellite altimetry*. PhD thesis, Ohio State University, Columbus, 2012.

L.-L. Fu and A. Cazenave, editors. *Satellite Altimetry and Earth Sciences: A Handbook of Techniques and Applications*. Academic Press, San Diego, California, 2001.

J. A. M. Green and J. Nycander. A comparison of internal wave-drag parameterizations for tidal model. *J. Phys. Oceanogr.*, 43:104–119, 2013. doi: 10.1175/JPO-D-12-023.1.

D. F. Hill, S. D. Griffiths, W. R. Peltier, B. P. Horton, and T. E. Törnqvist. High-resolution numerical modeling of tides in the western atlantic, gulf of mexico, and caribbean sea during the holocene. *J. Geophys. Res.*, 116(C10014), 2011. doi: 10.1029/2010JC006896.

S. R. Jayne and L. C. St. Laurent. Parameterizing tidal dissipation over rough topography. *Geophys. Res. Lett.*, 28(5):811–814, 2001.

A. Kuvshinov and N. Olsen. 3-D modelling of the magnetic fields due to ocean tidal flow. In C. Reigber, H. Lühr, P. Schwintzer, and J. Wickert, editors, *Earth Observation with CHAMP. Results from Three Years in Orbit*, pages 359–366. Springer-Verlag, Berlin, 2005.

F. Lyard, F. Lefevre, T. Letellier, and O. Francis. Modelling the global ocean tides: Modern insights from FES2004. *Ocean Dyn.*, 56:394–415, 2006.

P. J. Melchior. *The tides of the planet Earth*. Pergamon Press, Oxford, 2nd edition, 1983.

M. Müller, J. Y. Cherniawsky, M. G. G. Foreman, and J.-S. von Storch. Global map of M_2 internal tide and its seasonal variability from high resolution ocean circulation and tide modeling. *Geophys. Res. Lett*, 39(L19607), 2012. doi: 10.1029/2012GL053320.

R. D. Ray. Ocean self-attraction and loading in numerical tidal model. *Mar. Geod.*, 21 (3):181–192, 1998.

R. D. Ray. A global ocean tide model from Topex/Poseidon altimetry: GOT99.2. Technical report, Goddard Space Flight Center, Greenbelt, Maryland, 1999. NASA Tech. Memo. 209478.

R. D. Ray. Precise comparisons of bottom-pressure and altimetric ocean tides. *J. Geophys. Res. Oceans*, 118:4570–4584, 2013. doi: 10.1002/jgrc.20336.

T. J. Sabaka, N. Olsen, R. H. Tyler, and A. Kuvshinov. CM5, a pre-Swarm comprehensive geomagnetic field model derived from over 12 yr of CHAMP, Ørsted, SAC-C and observatory data. *Geophys. J. Int.*, 200:1596–1626, 2015. doi: 10.1093/gji/ggu493.

R. Savcenko and W. Bosch. EOT11a – Empirical ocean tide model from multi-mission satellite altimetry. Technical report, Deutsches Geodätisches Forschungsinstitut, München, 2012. DGFI Report No. 89.

M. Schindelegger, D. Einšpigel, D. Salstein, and J. Böhm. The global S_1 tide in Earth's nutation. *Surv. Geophys.*, 37(3):643–680, 2016. doi: 10.1007/s10712-016-9365-3.

M. Schindelegger, D. Salstein, D. Einšpigel, and C. Mayerhofer. Diurnal atmosphere-ocean signals in Earth's rotation rate and a possible modulation through ENSO. *Accepted to Geophys. Res. Lett.*, 2017. doi: 10.1002/2017GL072633.

G. Seeber. *Satellite Geodesy*. Walter de Gruyter, Berlin, Germany, 2nd edition, 2003.

A. F. Shchepetkin and J. C. McWilliams. The regional oceanic modeling system (ROMS): a split-explicit, free-surface, topography-following-coordinate oceanic model. *Ocean Model.*, 9:347–404, 2005.

A. F. Shchepetkin and J. C. McWilliams. Computational kernel algorithms for fine-scale, multi-process, long-time oceanic simulations. In R. Temam and J. Tribbia, editors, *Handbook of Numerical Analysis: Computational Methods for the Ocean and the Atmosphere*, pages 121–183. Elsevier Science, 2008. ISBN: 978-0-444-51893-4.

A. J. E. Smith. *Application of satellite altimetry for global ocean tide modeling*. PhD thesis, Delft University of Technology, Delft, 1999.

D. Stammer, R. D. Ray, O. B. Andersen, B. K. Arbic, W. Bosch, L. Carrère, Y. Cheng, D. S. Chinn, B. D. Dushaw, G. D. Egbert, S. Y. Erofeeva, H. S. Fok, J. A. M. Green, S. Griffiths, M. A. King, V. Lapin, F. G. Lemoine, S. B. Luthcke, F. Lyard, J. Morison, M. Müller, L. Padman, J. G. Richman, J. F. Shriver, C. K. Shum, E. Taguchi, and Y. Yi. Accuracy assessment of global barotropic ocean tide models. *Rev. Geophys.*, 52, 2014. doi: 10.1002/2014RG000450.

E. Taguchi, W. Zahel, and D. Stammer. Inferring deep ocean tidal energy dissipation from the global high-resolution data-assimilative HAMTIDE model. *J. Geophys. Res. Oceans*, 119:4573–4592, 2014.

R. S. Tyler, S. Maus, and H. Lühr. Satellite observations of magnetic fields due to ocean tidal flow. *Science*, 299:239–240, 2003.

J. Velímský, Z. Martinec, L. Šachl, D. Einšpigel, and L. Hanyk. Magnetic signatures of barotropic and baroclinic flows in Swarm data. Technical report, 2016. ESA Study Contract Report No. 4000109562/14/NL/CBi.

P. N. A. M. Visser, N. Sneeuw, T. Reubelt, M. Losch, and T. van Dam. Space-borne gravimetric satellite constellation and ocean tides: Aliasing effects. *Geophys. J. Int.*, 181:789–805, 2010.

V. Vlasenko, N. Stashchuk, and K. Hutter. *Baroclinic Tides: Theoretical Modeling and Observational Evidence*. Cambridge Univ. Press, Cambridge, U.K., 2005.

L. Šachl, D. Einšpigel, and Z. Martinec. Benchmark study of two tidal barotropic ocean models. *Submitted to Computat. Geosci.*, 2017.

P. Weis. *Ocean tides and the Earth's rotation – results of a high-resolving ocean model force by the lunisolar tidal potential*. PhD thesis, University of Hamburg, 2006.

P. Weis, M. Thomas, and J. Sündermann. Broad frequency tidal dynamics simulated by a high-resolution global ocean tide model forced by ephemerides. *J. Geophys. Res.*, 113(C10), 2008. doi: 10.1029/2007JC004556.

W. Zahel. Assimilating ocean tide determined data into global tidal models. *J. Mar. Syst.*, 6:3–13, 1995.

List of author's publications

Reviewed papers

- M. Schindelegger, D. Salstein, D. Einšpigel, and C. Mayerhofer. Diurnal atmosphere-ocean signals in Earth's rotation rate and a possible modulation through ENSO. *Accepted to Geophys. Res. Lett.*, 2017. doi: 10.1002/2017GL072633

- D. Einšpigel and Z. Martinec. Time-domain modelling of global ocean tides generated by the full lunisolar potential. *Ocean Dyn.*, 67(2):165–189, 2017. doi: 10.1007/s10236-016-1016-1

- M. Schindelegger, D. Einšpigel, D. Salstein, and J. Böhm. The global S_1 tide in Earth's nutation. *Surv. Geophys.*, 37(3):643–680, 2016. doi: 10.1007/s10712-016-9365-3

- D. Einšpigel and Z. Martinec. A new derivation of the shallow water equations in geographical coordinates and their application to the global barotropic ocean model (the DEBOT model). *Ocean Modelling*, 92:85–100, 2015. doi: 10.1016/j.ocemod.2015.05.006

- D. Einšpigel and L. Eisner. The differences in the detectability of perforation shots and microseismic events in the surface monitoring: the attenuation effect. *Acta Geodyn. Geomater.*, 11(2):159–164, 2014. doi: 10.13168/AGG.2013.0062

Technical report

- J. Velímský, Z. Martinec, L. Šachl, D. Einšpigel, and L. Hanyk. Magnetic signatures of barotropic and baroclinic flows in Swarm data. Technical report, 2016. ESA Study Contract Report No. 4000109562/14/NL/CBi

Submitted paper

- L. Šachl, D. Einšpigel, and Z. Martinec. Benchmark study of two tidal barotropic ocean models. *Submitted to Computat. Geosci.*, 2017